Radiation-pressure-dominant acceleration: Polarization and radiation reaction effects and energy increase in three-dimensional simulations

M. Tamburini,[1,2,*] T. V. Liseykina,[3] F. Pegoraro,[2,1] and A. Macchi[1,2]
[1]*Istituto Nazionale di Ottica, CNR, research unit "A. Gozzini," Pisa, Italy*
[2]*Dipartimento di Fisica "E. Fermi," Università di Pisa, Largo Bruno Pontecorvo 3, I-56127 Pisa, Italy*
[3]*Institut für Physik, Universität Rostock, D-18051 Rostock, Germany*
(Received 11 August 2011; published 30 January 2012)

Polarization and radiation reaction (RR) effects in the interaction of a superintense laser pulse ($I > 10^{23}$ W cm^{-2}) with a thin plasma foil are investigated with three dimensional particle-in-cell (PIC) simulations. For a linearly polarized laser pulse, strong anisotropies such as the formation of two high-energy clumps in the plane perpendicular to the propagation direction and significant radiation reactions effects are observed. On the contrary, neither anisotropies nor significant radiation reaction effects are observed using circularly polarized laser pulses, for which the maximum ion energy exceeds the value obtained in simulations of lower dimensionality. The dynamical bending of the initially flat plasma foil leads to the self-formation of a quasiparabolic shell that focuses the impinging laser pulse strongly increasing its energy and momentum densities.

DOI: 10.1103/PhysRevE.85.016407 PACS number(s): 52.38.Kd, 52.65.Rr

I. INTRODUCTION

The radiation pressure generated by ultraintense laser pulses may drive strong acceleration of dense matter, as experimentally shown in various regimes [1]. Thus, radiation pressure may be an effective mechanism for the generation of high-energy ions, especially in the regime of extremely high intensities and relativistic ion energies as foreseen with the ELI project. In the case of solid-density thin foil targets, pioneering particle-in-cell (PIC) simulations showed that at intensities exceeding 10^{23} W cm^{-2} and for linear polarization of the laser pulse radiation pressure dominates the acceleration yielding linear scaling with the laser pulse intensity, high efficiency and quasimonoenergetic features in the ion energy spectrum [2]. More recent two-dimensional (2D) simulations for a small disk target suggested a potentially "unlimited" energy gain for the fraction of ions that get phase locked with the laser pulse [3].

The above-mentioned studies showed that the radiation pressure dominant acceleration (RPDA) regime is very appealing as a route to the generation of relativistic ions, but they leave several theoretical issues open. First, transverse instabilities [4] and multidimensional effects may play a crucial role as shown by 2D simulations [3]. Second, the use of circular polarization (CP) instead of linear polarization (LP) quenches the generation of high-energy electrons [5], allowing radiation pressure to dominate even at intensities below 10^{23} W cm^{-2} and leading to efficient acceleration of ultrathin foils [6]; it has not been shown yet whether the use of CP is advantageous also at ultrahigh intensities ($I > 10^{23}$ W cm^{-2}), i.e., when the radiation pressure generated by the laser pulse becomes the dominant mechanism of acceleration both for CP and LP. Finally, it has been shown by one-dimensional (1D) simulations that radiation reaction (RR) effects may significantly affect the dynamics of radiation pressure acceleration both for thick [7] and thin targets [8,9], and also depend strongly on the polarization [8]. All of these phenomena may be affected by the dimensionality of the problem, and a fully three-dimensional (3D) approach is ultimately needed because, e.g., in 2D simulations and for LP the laser-plasma coupling is different for S and P polarization (i.e., for the electric field of the laser pulse either perpendicular or parallel to the simulation plane, respectively) and the constraint of the conservation of angular momentum carried by CP pulses holds in 3D only.

In this paper, we address the role of polarization and RR effects in the RPDA regime using fully 3D PIC simulations. To our knowledge, these are the first 3D simulations of ion acceleration in the RPDA regime with RR effects included and among the largest and most accurate 3D simulations reported so far. Our results show that even in the RPDA regime CP leads to higher ion energies and better collimation than LP, for which an anisotropic ion distribution is observed. It is also found that the bending of the foil leads to a self-generated parabolic shell that focuses the impinging pulse down to an almost λ^3 volume and that the energy density at the focus largely exceeds the initial peak energy density. Compared to 2D simulations with analogous parameters, the pulse focusing effect is remarkably enhanced and the cut-off energy of ions is increased. Radiation reaction effects on the ion spectrum are found to be negligible for CP but quite relevant for LP where they increase the energy cutoff.

II. MODELING AND SIMULATION SET-UP

Our approach is based on the numerical solution of kinetic equations for the phase-space distributions of electrons and ions, where RR is included in the motion of electrons via the Landau-Lifshitz (LL) force [10]. Details of our RR modeling and numerical implementation in a PIC code are given in Refs. [8,11]. The effective equation of motion for electrons, after neglecting terms that are negligible in the classical limit

*tamburini@df.unipi.it

 ©2012 American Physical Society

[8], is

$$\frac{d\mathbf{p}}{dt} = -e\left(\mathbf{E} + \frac{\mathbf{v}}{c} \times \mathbf{B}\right) + \mathbf{f}_R,$$
$$\mathbf{f}_R = \frac{2r_c^2}{3}\left\{ -\gamma^2\left[\left(\mathbf{E} + \frac{\mathbf{v}}{c} \times \mathbf{B}\right)^2 - \left(\frac{\mathbf{v}}{c} \cdot \mathbf{E}\right)^2\right]\frac{\mathbf{v}}{c} + \left[\left(\mathbf{E} + \frac{\mathbf{v}}{c} \times \mathbf{B}\right) \times \mathbf{B} + \left(\frac{\mathbf{v}}{c} \cdot \mathbf{E}\right)\mathbf{E}\right]\right\}, \quad (1)$$

where $r_c = e^2/m_e c^2$. The RR force contribution is important for ultrarelativistic electrons and it is usually dominated by the first term, while the second term ensures the on-shell condition [8]. Notice that the dominant term has almost the same form also in different approaches to RR modeling [7,9]. For a plane wave propagating along the x axis, the RR force is maximum or zero for counterpropagating ($v_x/c \to -1$) or copropagating ($v_x/c \to +1$) electrons, respectively.

In order to clarify the new qualitative features due to RR effects, we recall that the phase-space volume element J evolves according to $dJ/dt = J\nabla_{\mathbf{p}} \cdot \mathbf{f}_R$. It has been shown [11] that $\nabla_{\mathbf{p}} \cdot \mathbf{f}_R \leqslant 0$ and, therefore, the RR force leads to a *contraction* of the available phase-space volume. The physical interpretation of this property is that the RR force acts as a cooling mechanism for the system accounting for the emission of high-energy photons. These photons are assumed to escape from the plasma freely, carrying away energy and entropy [11].

We present a total of four 3D simulations each with the same physical and numerical parameters but different polarization, with and without RR effects. In these simulations, the laser field amplitude has a $\sin^2$-function longitudinal profile with 9λ full width at half-maximum (FWHM) (where $\lambda = 0.8\ \mu$m is the laser wavelength) while the transverse radial profile is Gaussian with 10λ FWHM and the laser pulse front reaches the edge of the plasma foil at $t = 0$. The peak intensity at the focus is $I = 1.7 \times 10^{23}$ W cm^{-2}, which corresponds to a normalized amplitude $a_0 = 280$ for LP and $a_0 = 198$ for CP. The target is a plasma foil of electrons and protons with uniform initial density $n_0 = 64 n_c$ (where $n_c = \pi m_e c^2/e^2\lambda^2$ is the critical density), thickness $\ell = 1\lambda$, and initially located in the region $10\lambda \leqslant x \leqslant 11\lambda$. The density $n_0 \simeq 1.1 \times 10^{23}$ cm^{-3} is slightly lower than that of solid targets but the areal density $n_0\ell$ has fully realistic values. Moreover, laser pulses of ultrahigh contrast are now available [[12], and references therein] to avoid early plasma formation effects by the prepulse, thus, a thin plasma with steplike profile is not an unrealistic assumption.

The simulation grid is $1320 \times 896 \times 896$ and the spatial step is $\lambda/44$ for each direction. The time step is $T/100$ where $T = \lambda/c = 2.67$ fs is the laser period. We use 216 particles per cell for each species and the total number of particles is 1.526×10^{10}. The runs were performed using 1024 processors each one equipped with 1.7 GB of memory of the IBM-SP6 cluster at the CINECA supercomputing facility in Bologna, Italy.

III. RESULTS AND DISCUSSION

Figure 1 shows the ion and the electron 3D spatial distributions [13] at $t = 20T$ for the LP case without (a) and with (b) RR and for the CP case without (c) and with (d) RR. The color (grayscale) corresponds to the range in kinetic energy. For CP, the ion spatial distribution follows the spatial intensity profile of the initial laser pulse, has rotational symmetry around the central axis, and a distribution in energy monotonically decreasing with increasing radial distance. The most energetic ions are located near the axis. The number of ions having energy $\mathcal{E} \geqslant 1100$ MeV and $\mathcal{E} \geqslant 800$ MeV are 2.3×10^{10} and 9.4×10^{10}, respectively. The electron spatial distribution has a helicoidal shape with step λ; Figs. 1(c),

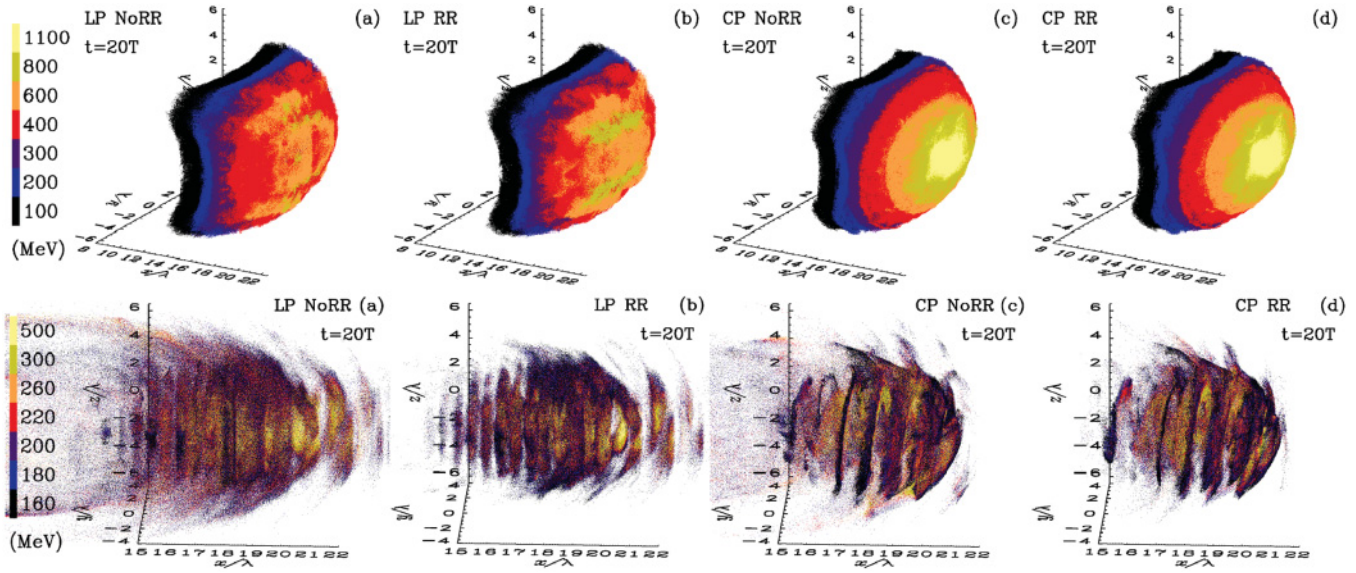

FIG. 1. (Color online) Spatial distributions of ions (upper row) and electrons (lower row) at $t = 20$ T and in the region $(|y|,|z|) \leqslant 5.7\lambda$, for LP without (a) and with (b) RR and for CP without (c) and with (d) RR. Ions and electrons are divided into seven populations according to their kinetic energy, with the color bar (grayscale) reporting the lower bound of the energy interval. In the LP case [(a) and (b)], the polarization is along the y axis.

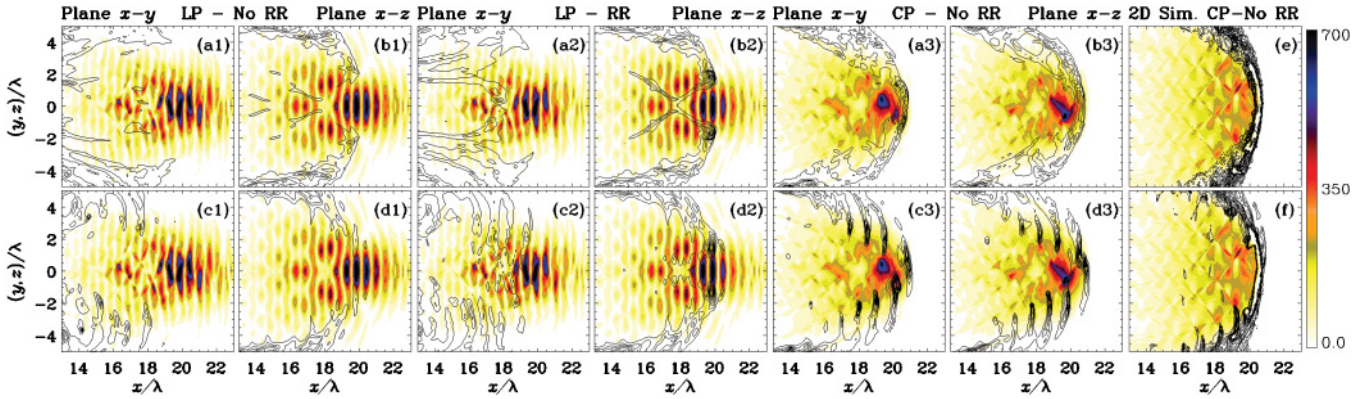

FIG. 2. (Color online) (x,y) and (x,z) sections of the 3D simulations of the laser pulse-foil interaction [(a1)–(a3), (b1)–(b3), (c1)–(c3), and (d1)–(d3)] and 2D simulations for CP and without RR with the same parameters as the 3D simulations [(e) and (f)], all at $t = 20T$. Each frame reports the color (grayscale) contours of $\sqrt{\mathbf{E}^2 + \mathbf{B}^2}$ (normalized units) in the xy plane at $z = 0$ [(a1)–(a3) and (c1)–(a3)], in the xz plane at $y = 0$ [(b1)–(b3) and (d1)–(d3)] and in the simulation plane [(e) and (f)] in the 2D case. Line contours of the ion and electron densities are superimposed in the upper and lower frames, respectively. The CP case with RR is almost identical to the CP case without RR and it is not reported.

and 1(d). Radiation reaction effects play a minor role for CP, affecting only a small fraction of ultrarelativistic electrons [mostly removing fast electrons *behind* the foil with almost no influence on the ion distribution as seen by comparing Figs. 1(c) and 1(d)].

The (x,y) and (x,z) sections of the total electromagnetic energy density and of the ion and electron densities for the CP case in Fig. 2 [(a3)–(b3) and (c3)–(d3)] evince a self-generated parabolic shell wrapping the laser pulse and focusing it up to nearly a λ^3 volume, so both the energy and the momentum densities at the focus reach values more than 8 times their peak value in the initial laser pulse. This effect is much weaker in 2D simulations with the same parameters as shown in Figs. 2(e)–2(f). Along the axis, the peak value and width of the ion density profile are $\simeq 10 n_c$ and $\simeq 0.5\lambda$, showing a strong rarefaction due to the transverse expansion, potentially leading to enhanced acceleration as described in Ref. [3].

For LP, the peak ion energy is lower than for CP, the ion distribution is anisotropic, and RR effects are much stronger. The most energetic ions (800–1100 MeV) are grouped into two off-axis clumps lengthened and aligned along the polarization direction, and their number is increased in the case with RR as seen by the comparison of Figs. 1(a) and 1(b) and also in Figs. 2 [(a1),(a2) and (b1),(b2)] where sections of the ion density in the (x,y) and (x,z) planes are shown. The contours of the electromagnetic (EM) energy density in Figs. 2 [(a1),(a2) and (b1),(b2)] show that near the axis most of the laser pulse has been transmitted through the target. The increased bunching and higher density observed in the case with RR may be related to the higher ion energies since the local increase of the density and, therefore, of the reflectivity leads to a longer and more efficient RPDA phase. This is consistent with observing in Figs. 2(b1) and 2(b2) that the EM energy density is higher behind the two high-density clumps, which correspond to the most energetic ions and are similar to the ion lobes observed in Ref. [14] at lower intensity and in a regime of strong pulse penetration through the foil. The pulse focusing effect by the self-generated parabola is present also in the LP case although weaker than in the CP case and presumably reduced as the laser pulse breaks through the parabolic shell.

The differences between CP and LP in the acceleration dynamics are well explained, for planar geometry and nonrelativistic ions, by the absence of the oscillating component of the $\mathbf{J} \times \mathbf{B}$ force for CP [5], which maximizes the effect of the radiation pressure strongly suppressing the electron heating. The absence of the oscillating component of the $\mathbf{J} \times \mathbf{B}$ force also accounts for the very different RR effects. For CP, a steady push of the foil and weak pulse penetration are observed and most of the electrons move coherently with the foil and in the same direction as the laser pulse so the RR force becomes very small in accordance with Eq. (1) since the electrons effectively copropagate with the laser pulse (see also Refs. [2,8]). For LP, the $\mathbf{J} \times \mathbf{B}$-driven oscillations allow electrons to collide with the counterpropagating laser pulse twice per cycle producing temporal maxima in the RR force in agreement with Eq. (1). Our present results indicate that CP leads to more efficient acceleration, producing higher energy and collimated ion beams, and making RR effects negligible also in the 3D case, accounting for target bending and pulse focusing effects, and for relativistic ions.

Large-scale 3D PIC simulations are limited by the size and availability of computational resources both in the number of runs that may be performed and in the achievable numerical resolution. This last issue may raise doubts on the accuracy of 3D results. To gain confidence on this side, as well as to compare the 3D results to those obtained in lower dimensionality, we performed 2D simulations both with numerical parameters similar to those of 3D runs and with higher resolution. The effect of increasing resolution and particle number on the ion spectra in 2D simulations is shown in Fig. 3 where 2D results are reported for the three different polarization cases (CP, LP-S, and LP-P) and compared with the 3D results for both LP and CP. The spectra are normalized to unity both in the 2D and 3D cases. In the CP case both numerical and RR effects on the spectrum are smaller while in the P-polarization case these effects are larger. Changing the spatial resolution from $\lambda/44$ to $\lambda/80$ and increasing the number of particles-per-cell for each species from 256 to 625 shifts the energy cutoff by $\sim$2% in the CP case and by $\sim$15% ($\sim$20%) in the P-polarization case without RR (with RR). The stronger

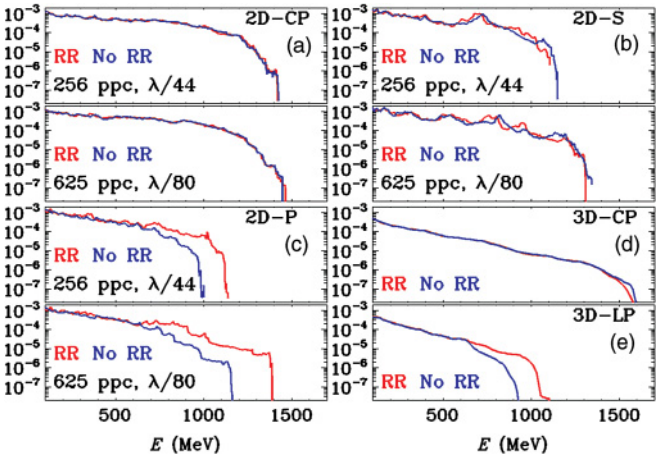

FIG. 3. (Color online) Ion spectra from 2D [(a)–(c)] and 3D [(d)–(e)] simulations with same physical parameters, all at $t = 20T$. The 2D spectra are reported for circular [CP, panel (a)] and linear (LP) "S" [panel (b)] and "P" [panel (c)] polarization cases. In each plot, the blue (dark gray) and red (light gray) curves correspond to simulations without and with radiation reaction (RR) effects, respectively. In the upper plots of panels (a)–(c) the numerical resolution (number of particles per cell and of points per wavelength) is similar to those of the 3D simulations in panels (d) and (e), while in the lower plots the results for higher resolution are shown.

effect of the inclusion of RR for the higher resolution case may be explained by noticing that RR mostly affects the highest energy electrons [8], which are located in the high-energy tail of the distribution function that needs a very large number of particles to be resolved properly. Nevertheless, the limited resolution does not qualitatively affect prominent features in ion spectra, such as the higher ion energy for CP and the relevance of RR effects for LP only, leading for this latter case to an *higher* energy of ions with respect to the case of no RR as observed in 1D simulations [8]. As a novel feature of 2D simulations, P polarization leads to much stronger RR effects than S polarization. In fact, for P polarization the electric field can drag a large fraction of electrons out in vacuum and toward the laser pulse as the plasma foil begins to bend, enhancing the RR effect.

For CP, the maximum ion energy is higher in the 3D case ($\simeq$1600 MeV) than in the 2D case ($\simeq$1400 MeV). In turn, the latter value is higher than what found in 1D, plane-wave simulations, for which we find a broad spectral peak which at $t = 20$ extends up to $\simeq$1100 MeV and is centered around a value of $\simeq$870 MeV. The latter value corresponds to the energy $\mathcal{E}_{\rm LS} = (\gamma - 1)m_p c^2$, where $\gamma = 1/\sqrt{1-\beta^2}$ and β are obtained from the "light sail" model [[15], and references therein] by numerically integrating the 1D equations of motion for the foil

$$\frac{d\gamma\beta}{dt} = \frac{2I(t - X/c)}{n_0 \ell m_p c^2}\left(\frac{1-\beta}{1+\beta}\right), \qquad \frac{dX}{dt} = \beta c. \tag{2}$$

From the 1D modeling we also evaluate a final ion energy for the spectral peak of $\simeq$1700 MeV that is reached at $t \simeq 90$. The 3D simulations could not be extended up to the end of the acceleration stage (estimated up to $\sim 90T$ in 1D simulations) but, since the efficiency of RPDA increases with the foil velocity, the energy gain is expected to be even larger at the later times (provided that 3D effects do not cause an early stop of the acceleration). Hence, the comparison at $t = 20$ shows an overall *increase* of the ion energy in the 3D case with respect to 1D and 2D cases. Part of the energy enhancement can be attributed to the reduction of the areal density $n_0\ell$ due to the transverse expansion, as was noticed in 2D simulations supporting the model of "unlimited" acceleration [3]. An additional contribution may come from the above-described focusing of the laser pulse by the deformed foil, which is stronger in 3D geometry. This latter effect was absent in the simulations of Ref. [3] because a target with a radius smaller than the pulse waist was considered.

IV. CONCLUSIONS

In conclusion, with three-dimensional particle-in-cell simulations of ultraintense laser interaction with solid-density foils we showed that circular polarization improves ion acceleration also in the radiation pressure dominant regime, confirming and extending previous results obtained for lower intensity and/or lower dimensionality. In detail, circular polarization leads to the highest ion energies, to a symmetrical and collimated distribution, and to negligible effects of radiation reaction. In addition, the maximum energy of ions in 3D is larger than observed in corresponding 1D and 2D simulations. This enhancement is attributed both to the density decrease in the target, as noticed in the "unlimited acceleration" model [3], and to the strong focusing of the laser pulse by the parabolically deformed foil. In the linear polarization case, lower maximum energies are achieved, the most energetic ions are grouped anisotropically into two off-axis clumps and radiation reaction effects significantly affect the energy spectrum. We expect these findings to be of relevance for the design of future experiments on laser acceleration of ions up to relativistic (GeV) energy.

ACKNOWLEDGMENTS

Work sponsored by the Italian Ministry of University and Research via the FIRB project "SULDIS." We acknowledge the CINECA Grant No. HP10A25JKT-2010 for the availability of high-performance computing resources.

[1] S. Kar *et al.*, Phys. Rev. Lett. **100**, 225004 (2008); K. U. Akli *et al.*, *ibid.* **100**, 165002 (2008); A. Henig *et al.*, *ibid.* **103**, 245003 (2009); C. A. J. Palmer *et al.*, *ibid.* **106**, 014801 (2011).

[2] T. Esirkepov, M. Borghesi, S. V. Bulanov, G. Mourou, and T. Tajima, Phys. Rev. Lett. **92**, 175003 (2004).

[3] S. V. Bulanov, E. Y. Echkina, T. Z. Esirkepov, I. N. Inovenkov, M. Kando, F. Pegoraro, and G. Korn, Phys. Rev. Lett. **104**, 135003 (2010)

[4] F. Pegoraro and S. V. Bulanov, Phys. Rev. Lett. **99**, 065002 (2007).

[5] A. Macchi, F. Cattani, T. V. Liseykina, and F. Cornolti, Phys. Rev. Lett. **94**, 165003 (2005).

[6] X. Zhang, B. Shen, X. Li, Z. Jin, and F. Wang, Phys. Plasmas **14**, 073101 (2007); A. P. L. Robinson, M. Zepf, S. Kar, R. G. Evans, and C. Bellei, New J. Phys. **10**, 013021 (2008); O. Klimo, J. Psikal, J. Limpouch, and V. T. Tikhonchuk, Phys. Rev. ST Accel. Beams **11**, 031301 (2008).

[7] N. Naumova, T. Schlegel, V. T. Tikhonchuk, C. Labaune, I. V. Sokolov, and G. Mourou, Phys. Rev. Lett. **102**, 025002 (2009).

[8] M. Tamburini, F. Pegoraro, A. D. Piazza, C. H. Keitel, and A. Macchi, New J. Phys. **12**, 123005 (2010).

[9] M. Chen, A. Pukhov, T.-P. Yu, and Z.-M. Sheng, Plasma Phys. Contr. Fusion **53**, 014004 (2011).

[10] L. D. Landau and E. M. Lifshitz, *The Classical Theory of Fields*, 2nd ed. (Elsevier, Oxford, 1975).

[11] M. Tamburini, F. Pegoraro, A. D. Piazza, C. Keitel, T. Liseykina, and A. Macchi, Nucl. Inst. Methods A **653**, 181 (2011).

[12] C. Thaury *et al.*, Nat. Phys. **3**, 424 (2007); C. Rödel, M. Heyer, M. Behmke, M. Kübel, O. Jäckel, W. Ziegler, D. Ehrt, M. Kaluza, and G. Paulus, Appl. Phys. B: Lasers Opt. **103**, 295 (2011).

[13] See Supplemental Material at http://link.aps.org/supplemental/10.1103/PhysRevE.85.016407 for high-quality pictures of the three-dimensional electron and ion spatial distributions reported in Fig. 1.

[14] L. Yin, B. J. Albright, K. J. Bowers, D. Jung, J. C. Fernández, and B. M. Hegelich, Phys. Rev. Lett. **107**, 045003 (2011).

[15] A. Macchi, S. Veghini, T. V. Liseykina, and F. Pegoraro, New J. Phys. **12**, 045013 (2010).